Current **A**pplied **S**cience and **T**echnology e-ISSN: 2586-9396

Curr. Appl. Sci. Technol. 2025, Vol. 25 (No. 6), e0265240

Research article

Effect of Dopant Gas Sources on the Properties of Boron Doped p-a-$Si_{1-x}O_x$:H Films and Their Application to a-$Si_{1-x}O_x$:H Thin Film Solar Cells

Sorapong Inthisang[1]* and Kobsak Sriprapha[2]

[1]Division of Physics, Faculty of Science, Nakhon Phanom University, Nakhon Phanom, Thailand
[2]Solar Energy Technology Laboratory (STL), National Electronics and Computer Technology Center (NECTEC), Pathumthani, Thailand

Received: 5 November 2024, Revised: 19 February 2025, Accepted: 6 March 2025, Published: 8 May 2025

Abstract

Hydrogenated amorphous silicon (a-Si:H) thin-film solar cells offer low-cost production and flexibility, making them promising for renewable energy applications. This study examined the effects of the dopant gases diborane (B_2H_6), trimethyl boron (TMB), and a B_2H_6 + TMB combination on the optical and electrical properties of boron-doped hydrogenated amorphous silicon oxide (p-a-$Si_{1-x}O_x$:H) films for window layers in a-Si:H solar cells. Films were fabricated using very high frequency plasma-enhanced chemical vapor deposition (VHF-PECVD), optimizing doping concentrations to balance a high optical bandgap (E_{opt}) and conductivity. TMB-doped films exhibited higher E_{opt} and better optical properties, while the B_2H_6 + TMB combination improved conductivity and overall performance. Single-junction a-$Si_{1-x}O_x$:H cells with mixed-doping window layers achieved superior open-circuit voltage (V_{oc}), fill factor (FF), and quantum efficiency (QE) compared to cells doped solely with B_2H_6 or TMB. These enhancements were attributed to improved interface quality between the window and absorber layers. The findings highlight the advantages of a mixed-doping approach, which optimizes optical and electrical properties, resulting in more efficient and stable thin-film solar cells. This work provides a pathway for developing high-performance and cost-effective photovoltaic devices.

Keywords: hydrogenated amorphous silicon oxide; doping gas; boron doping; TMB

1. Introduction

The increasing global demand for renewable energy sources has intensified interest in photovoltaic technologies (Daugaard et al., 2020; Calise et al., 2021; Yadav et al., 2023; Macías et al., 2024). Among the available options, hydrogenated amorphous silicon (a-Si:H) thin-film solar cells have emerged as a promising solution due to their low production costs, energy-efficient manufacturing process, and design flexibility (Wijewardane & Kazmerski, 2023). Compared to conventional crystalline silicon solar cells, a-Si:H cells

*Corresponding author: E-mail: sorapong.inthisang@npu.ac.th
https://doi.org/10.55003/cast.2025.265240

require significantly less material, reducing production complexity and minimizing environmental impact. Their compatibility with flexible substrates further makes them suitable for portable electronics and building-integrated photovoltaics (BIPV) (Lim et al., 2014; Kim et al., 2018).

A typical single-junction a-Si:H thin-film solar cell features a p-i-n structure consisting of a p-type layer, an intrinsic (i) layer, and an n-type layer. The intrinsic layer serves as the primary absorber, generating electron-hole pairs upon sunlight exposure, while the p-type and n-type layers facilitate charge separation and collection. However, single-junction cells often face limitations in conversion efficiency. To address this, tandem structures stack multiple p-i-n cells to capture a broader range of the solar spectrum. These designs typically pair a-Si:H with microcrystalline silicon (μc-Si) to enhance both stability and efficiency. Further advancements include triple-junction structures, which integrate three stacked layers, each optimized to absorb different regions of the solar spectrum. These multi-junction architectures reduce energy losses and increase power conversion efficiency by expanding the range of usable wavelengths (Kim et al., 2013; 2015; Schüttauf et al., 2015).

The p-layer plays a crucial role in determining the overall conversion efficiency of a-Si thin-film solar cells. A wide-bandgap p-layer with excellent electrical properties allows greater sunlight transmission to the intrinsic layer, boosting the short-circuit current (J_{SC}). Simultaneously, the wide bandgap increases the built-in potential (V_b), enhancing the open-circuit voltage (V_{OC}). Additionally, the p-layer's conductivity influences the fill factor (*FF*), further affecting the overall efficiency of the solar cell.

Given the importance of these properties, various materials have been explored for wide-bandgap p-layers. Hydrogenated amorphous silicon carbide (p-a-$Si_{1-x}C_x$:H) and microcrystalline silicon carbide (p-μc- $Si_{1-x}C_x$:H) have received significant attention (Myong et al., 2002; 2004; Sánchez et al., 2011). Additionally, boron-doped hydrogenated amorphous silicon oxide (p-a-$Si_{1-x}O_x$:H) has emerged as a promising alternative (Fujikake et al., 1994; Matsumoto et al., 2001). Diborane (B_2H_6) is a widely used dopant gas for p-a-$Si_{1-x}O_x$:H films and is also employed in the preparation of p-a-$Si_{1-x}C_x$:H and p-μc-$Si_{1-x}C_x$:H (Lim et al., 2014; Kim et al., 2018; Wijewardane & Kazmerski, 2023). For microcrystalline silicon oxide (p-μc-$Si_{1-x}O_x$:H) and microcrystalline silicon (p-μc-Si), trimethyl boron (TMB) and boron trifluoride (BF_3) are alternative dopants (Kumar et al., 2006; Lambertz et al., 2012; Krajangsang et al., 2013). However, BF_3 is often avoided due to its tendency to release fluorine gas (F_2), causing corrosion in vacuum systems.

For p-a-$Si_{1-x}O_x$:H and p-μc- $Si_{1-x}O_x$:H, carbon dioxide (CO_2) has emerged as a viable source of oxygen atoms for a-Si:H films, offering a cost-effective and environmentally friendly method for incorporating oxygen into the film matrix. The incorporation of oxygen atoms significantly influences the optical and electrical properties of a-Si:H films, particularly by modifying the optical bandgap (E_{opt}). Oxygen atoms bond with silicon, disrupting the amorphous network and increasing disorder, which results in a widening of the bandgap (Otsubo et al., 1988). This effect is crucial for tailoring material properties to specific photovoltaic applications, as a higher E_{opt} enhances the transmission of shorter-wavelength light to the intrinsic layer, improving overall solar cell performance (Staebler & Wronski, 1977).

The oxygen content in a-Si:H films plays a key role in determining their E_{opt} values. Higher oxygen content generally leads to an increase in the bandgap, but excessive oxygen can degrade the film's electrical properties by introducing localized states within the bandgap. These states trap charge carriers, reducing conductivity and negatively impacting solar cell efficiency. Therefore, optimizing oxygen content is essential to strike a

balance between enhanced optical properties and minimized electrical losses, as well as controlling the doping gas.

While most conventional a-Si:H solar cells utilize a single dopant gas for p-layer deposition, this study explores a new doping method that combines B_2H_6 and TMB. The films are deposited under conditions near the amorphous-to-microcrystalline phase transition, with preliminary results showing conversion efficiencies exceeding 8.0% for single-junction a-Si:H solar cells (Sriprapha et al., 2011). Despite the potential of B_2H_6, TMB, and BF_3 as dopants, a systematic comparison of films deposited at identical doping concentrations is lacking. Furthermore, the effect of these dopant gases on the electrical and optical properties of wide-bandgap p-a-$Si_{1-x}O_x$:H films remains underexplored.

This paper investigates the electrical and optical properties of boron-doped p-a-$Si_{1-x}O_x$:H films, comparing the results of using different dopant gases at identical doping concentrations. The study also evaluates the material quality and performance of these films through the fabrication of a-$Si_{1-x}O_x$:H single-junction solar cells, offering insights into how dopant selection influences solar cell efficiency.

2. Materials and Methods

2.1 Preparation of p-a-$Si_{1-x}O_x$:H films

The p-a-$Si_{1-x}O_x$:H films were deposited onto Corning 7059 glass substrates using very high frequency plasma-enhanced chemical vapor deposition (VHF-PECVD) at a plasma frequency of 40 MHz. The deposition chamber was maintained at a pressure of approximately 10^{-6} Torr using a turbomolecular pump backed by rotary pumps. Silane (SiH_4), hydrogen (H_2), and carbon dioxide (CO_2) were used as gas sources, with B_2H_6 (1% in H_2), TMB (3% in H_2), and a mixture of B_2H_6 + TMB employed as doping sources. The doping concentration for each dopant was calculated based on the ratio of doping gas to SiH_4, with a 1:1 ratio for the B_2H_6 + TMB mixture.

The film thickness was maintained at 20 nm. Deposition conditions for p-a-$Si_{1-x}O_x$:H films are summarized in Table I. Dark conductivity (σ_d) was measured using an aluminum (Al) coplanar electrode configuration at room temperature.

Table1. Deposition conditions for p-a-$Si_{1-x}O_x$:H films

Substrate temperature (°C)	180
Deposition pressure (mTorr)	500
Power density (mW/cm^2)	33.3
SiH_4 (sccm)	20.0
CO_2 (sccm)	10.0
H_2 (sccm)	200
B_2H_6 1% in H_2 (sccm)	0.4 – 4.0
TMB 3% in H_2 (sccm)	0.6 – 1.6

2.2 Optical and electrical properties characterization of p-a-$Si_{1-x}O_x$:H films

The optical bandgap (E_{opt}) and film thickness were determined via spectroscopic ellipsometry (J.A. Woollam, V-VASE series), with data analysis conducted using the Tauc-Lorentz model (von Blanckenhagen et al., 2002).

The film thickness was maintained at 20 nm. Dark conductivity (σ_d) was measured using an aluminum (Al) coplanar electrode configuration at room temperature. The measurement of the σ_d of the p-a-$Si_{1-x}O_x$:H configuration is shown in Figure 1.

An electric voltage V can be applied between the two-contact pad and the resulting electrical current, as represented by $I = A$ x J, can be measured. Here, J is the current density and A is the cross-section of the p-a-$Si_{1-x}O_x$:H films through which the current is flowing.

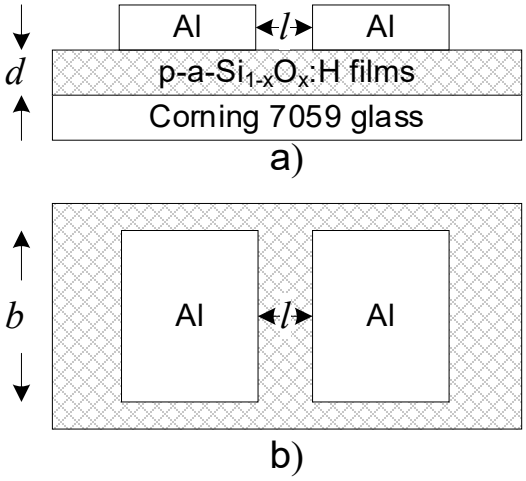

Figure 1. Experimental structure of co-planar conductivity measurement a) cross-sectional view; b) top view

From Figure 1, A is the product of the thickness d of the p-a-$Si_{1-x}O_x$:H film and the side length b of the contact pad. When a voltage V is applied to the contact pad, provided the contacts are ohmic, an electric field $E = V/l$ is created. This will lead to a current density:

$$J = \sigma E = J_n + J_p \tag{1}$$

or:

$$J = (q\mu_n n + q\mu_p p)E \tag{2}$$

$$\sigma = (q\mu_n n + q\mu_p p) = \sigma_n + \sigma_p \tag{3}$$

In this context, σ represents the conductivity of the p-a-$Si_{1-x}O_x$:H film, where σ_n accounts for the portion of conductivity due to electrons, and σ_p represents the portion due to holes (Shah, 2010).

2.3 Fabrication of a-$Si_{1-x}O_x$:H single-junction solar cells

In a-Si:H solar cells, tin oxide (SnO_2) and zinc oxide doped with aluminum (ZnO:Al) play essential roles in optimizing performance. SnO_2, a transparent conducting oxide (TCO), is widely used in the superstrate structure, where light enters through a glass substrate coated with SnO_2. This material serves as a transparent front electrode due to its high optical transparency, good electrical conductivity, and wide bandgap of approximately 3.6-4.0 eV, ensuring minimal absorption of visible light. Additionally, its textured surface scatters incoming light, increasing the optical path length within the active silicon layer, thereby enhancing light absorption and efficiency. SnO_2 is also stable, cost-effective, and compatible with large-scale manufacturing, making it a commercially viable choice. The a-$Si_{1-x}O_x$:H single-junction solar cells were fabricated on Asahi type U SnO_2 glass with the TCO material thickness of around 800 nm and the size of this glass was 10 cm^2 (Chen et al., 2012). The structure of the cell consisted of SnO_2 glass /seed layer/p-a-$Si_{1-x}O_x$:H /i-a-$Si_{1-x}O_x$:H buffer layer/ i-a-$Si_{1-x}O_x$:H absorbing layer/(n-type microcrystalline silicon) n-µc-Si:H/Zinc oxide doped aluminum ZnO:Al/(Silver) Ag/(aluminum) Al structure. ZnO:Al, Ag and Al back electrodes were deposited by magnetron sputtering. The ZnO:Al is commonly used as a back contact in amorphous silicon solar cells, where it functions as a transparent conductive layer and enhances light reflection when paired with a reflective metal layer like silver or aluminum. With a bandgap of about 3.3 eV, ZnO:Al maintains transparency while its aluminum doping improves electrical conductivity. Its textured surface further aids in light trapping, increasing absorption in the active layer. The thicknesses of the p, buffer, i and n layers were kept constant at 20, 10, 300 and 40 nm, respectively. A laser cutter was used to cut the cells to the active area of 1 cm^2.

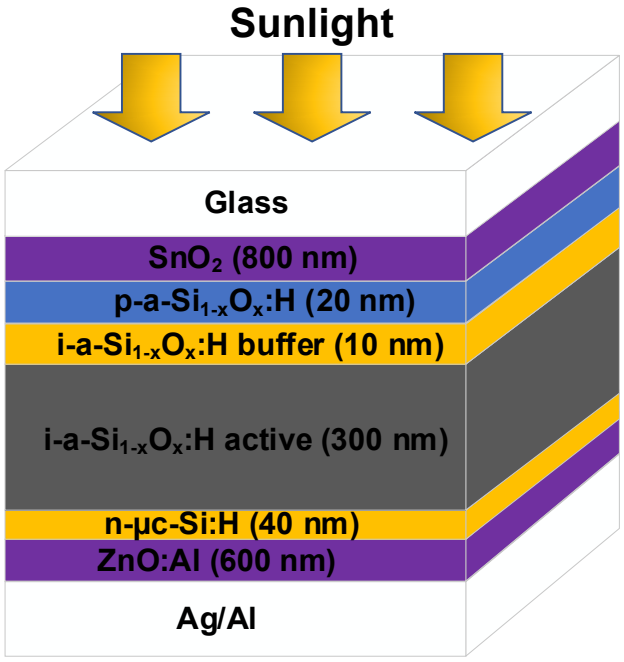

Figure 2. Experimental structure of a-$Si_{1-x}O_x$:H single-junction solar cell

2.4 Characterization of a-$Si_{1-x}O_x$:H single-junction solar cells

The photovoltaic (PV) parameters of single-junction solar cells were investigated following equation (4) under standard test conditions of AM 1.5 and 100 mW/cm^2 at 25°C using the solar simulator (Wacom, model WXS-155S-L2). The quantum efficiency (QE) of the solar cells was characterized using a quantum efficiency measurement system (PV Measurement, QEW7).

$$E_{ff} = \frac{J_{sc}\ x\ V_{oc}\ x\ FF}{P_{in}} x100\% \quad (4)$$

Here; E_{ff} is the solar cell conversion efficiency, J_{sc} is the short circuit current density, V_{oc} is open-circuit voltage, FF is the fill factor, and P_{in} is the light source intensity under the standard condition.

3. Results and Discussion

3.1 Optimization of p-a-$Si_{1-x}O_x$:H films

The primary goal of this experiment was to prepare high-quality, wide-bandgap p-type p-a-$Si_{1-x}O_x$:H films with E_{opt} of 2.0 eV and a σ_d of approximately 10^{-6} S/cm (Ichikawa et al., 1991). This was achieved by adjusting the dopant gas source concentrations. Figures 3 and 4 illustrate the relationship between E_{opt} and σ_d as a function of dopant gas concentration for p-a-$Si_{1-x}O_x$:H films. For films doped with B_2H_6, as the concentration increased from 1800 to 4200 ppm, the E_{opt} of p-a-$Si_{1-x}O_x$:H decreased significantly from 2.0 eV to 1.77 eV. This decrease suggests that the optical bandgap was reduced with greater boron incorporation into the a-$Si_{1-x}O_x$:H matrix (Calise et al., 2021; Wijewardane et al.,2023). In contrast, σ_d increased from 1.2 × 10^{-7} to 2.2 × 10^{-6} S/cm as the B_2H_6 concentration rose, indicating improved conductivity with higher doping levels.

In comparison, TMB showed an inverse trend. The E_{opt} of TMB-doped films increased slightly from 1.99 eV to 2.03 eV as the TMB concentration increased, likely due to the presence of carbon in TMB, which enhances the optical properties of films. However, σ_d declined from 3.4 × 10^{-6} to 4.2 × 10^{-7} S/cm, possibly due to increased C alloying, which raised the insulation level and defect density within the films. TMB-doped films exhibited improved optical properties at the target E_{opt} of around 2.0 eV compared to B_2H_6-doped films. Therefore, using a mixture of B_2H_6 and TMB as the dopant gas could potentially enhance p-a-$Si_{1-x}O_x$:H film quality. With this mixture, E_{opt} slightly decreased from 2.01 to 1.98 eV, while σ_d progressively rose from 3.3 × 10^{-6} to 5.2 × 10^{-6} S/cm as the combined concentration of TMB and B_2H_6 increased from 1800 to 4200 ppm. At lower doping levels (<3000 ppm), TMB-doped films and films doped with the mixture showed similar optical and electrical properties. However, at higher concentrations (>3000 ppm), the B_2H_6 + TMB mixture provided superior electrical properties while only slightly diminishing the optical characteristics.

The deposition rate for all dopant gases (Figure 5) showed a linear increase with higher doping concentrations, though films produced with the mixed gas exhibited a lower deposition rate (0.01 nm/s) than those deposited with only B_2H_6 or TMB.

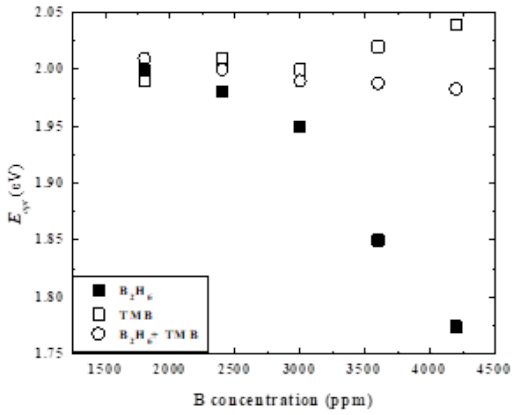

Figure 3. E_{opt} of p-a-$Si_{1-x}O_x$:H as a function of dopant gas source concentration

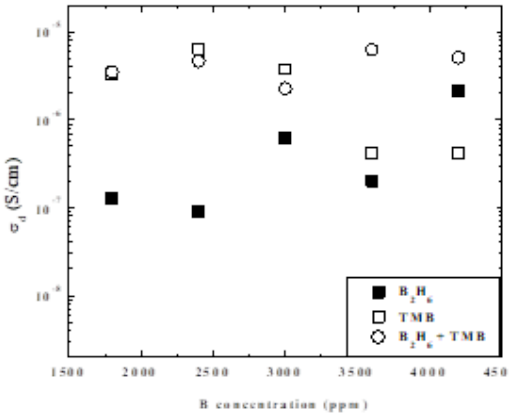

Figure 4. Dark conductivity (σ_d) of p-a-$Si_{1-x}O_x$:H as a function of dopant gas source concentration

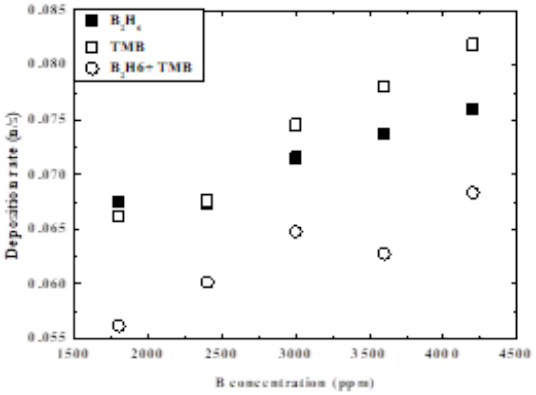

Figure 5. Deposition rate of p-a-$Si_{1-x}O_x$:H deposited with different dopant gas source concentration

3.2 Fabrication of p-a-$Si_{1-x}O_x$:H single – junction solar cells

To evaluate the quality of p-a-$Si_{1-x}O_x$:H films deposited with various dopant gases, a-$Si_{1-x}O_x$:H single-junction solar cells were fabricated. The window layer's optical bandgap was consistently maintained at approximately 2.0 eV (Figure 6).

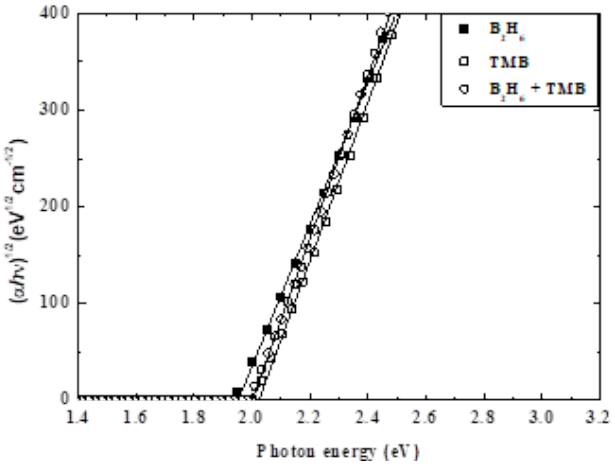

Figure 6. Optical bandgap (E_{opt}) of the p-a-$Si_{1-x}O_x$:H films deposited with varying concentrations of different dopant gases, used in the evaluation and fabrication a-$Si_{1-x}O_x$:H single-junction solar cells

Table 2 and Figure 7 illustrate the performance of a-$Si_{1-x}O_x$:H single-junction solar cells fabricated with different gas doping types for the window layer. The results indicate that cells doped with TMB and TMB + B_2H_6 achieved a high V_{oc} of 0.98 V, while cells doped exclusively with B_2H_6 exhibited a lower V_{oc} of 0.94 V. This finding aligns with the optical bandgap of the films, as shown in Figure 3, which demonstrates that using a wider bandgap window layer leads to a higher V_{oc}, corresponding to a higher effective built-in potential (V_b)

However, a higher V_{oc} is not solely dependent on the bandgap of the window layer; it also depends on the electrical properties of this layer. Figure 4 shows that, at the same doping concentration of 3000 ppm corresponding to an E_{opt} of approximately 2.0 eV, the film doped with pure B_2H_6 exhibited the lowest σ_d.

Furthermore, since the efficiency (E_{ff}) of the solar cell depends on V_{oc}, as shown in equation (4), the solar cells doped with pure B_2H_6 demonstrated the lowest efficiency, as indicated in Table 2 and Figure 7.

In terms of J_{sc}, cells with the TMB + B_2H_6-doped window layers displayed the best performance. To explore this further, quantum efficiency measurements were conducted. Figure 8 shows the quantum efficiency of a-$Si_{1-x}O_x$:H single-junction solar cells with varying gas doping types in the window layer. It was observed that cells doped with B_2H_6 exhibited the highest light absorption in the short-wavelength region compared to those doped with TMB and TMB + B_2H_6. Meanwhile, the mixture of TMB + B_2H_6 showed the lowest loss in the short-wavelength region. This result suggests that using a mixture of TMB + B_2H_6 for gas doping in the window layer can lead to higher solar cell efficiency, as it results in a higher J_{sc} compared to solar cells fabricated using conventional gas doping methods, such

Table 2. Deposition conditions for p-a-$Si_{1-x}O_x$:H films

	Solar Cell Parameters			
Doping Gas	V_{oc} (V)	J_{sc} (mA/cm^2)	*FF*	E_{ff} (%)
B_2H_6				
Cell A	0.93	11.15	0.60	6.6
Cell B	0.95	11.47	0.64	7.0
Cell C	0.98	11.81	0.68	7.4
TMB				
Cell A	0.94	11.64	0.63	7.2
Cell B	0.95	11.9	0.67	7.5
Cell C	0.96	12.13	0.69	7.9
B_2H_6 +TMB				
Cell A	0.95	11.87	0.62	7.6
Cell B	0.96	12.42	0.67	8.0
Cell C	0.98	12.98	0.71	8.4

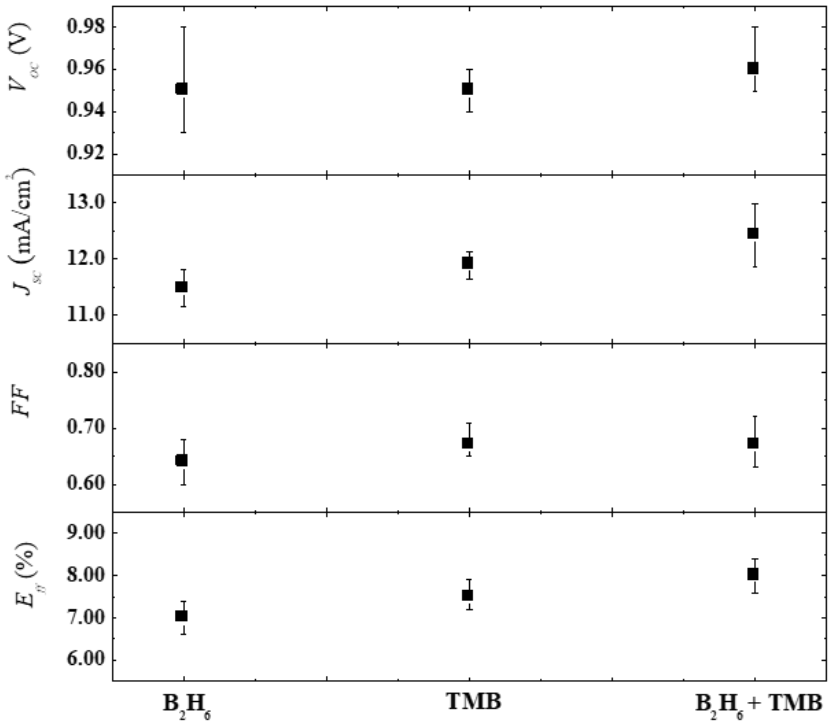

Figure 7. Performance of a-$Si_{1-x}O_x$:H single-junction solar cells fabricated with different gas doping types for the window layer

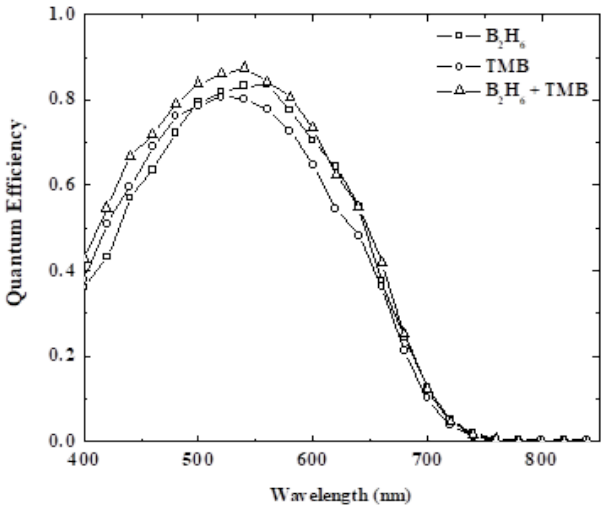

Figure 8. External quantum efficiency of a-$Si_{1-x}O_x$:H single-junction solar cells fabricated with different gas doping types for the window layer

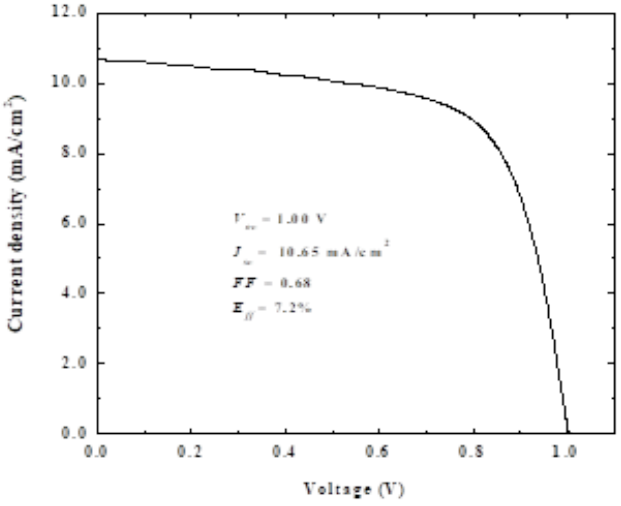

Figure 9. *J-V* characteristic of the highest V_{oc} of a-$Si_{1-x}O_x$:H single-junction solar cells fabricated with TMB + B_2H_6 gas doping types for the window layer

as pure B_2H_6 or TMB. The TMB + B_2H_6-doped cells demonstrated the highest J_{sc} due to their reduced light absorption across all regions compared to cells with pure TMB or B_2H_6 doping. It is important to note that J_{sc} in solar cells is influenced not only by the optical properties of the window layer but also by the quality of the interface between the window and the absorber layer (p/i interface). The experimental results indicate that the new TMB + B_2H_6 gas mixture for window layer doping enhances both the quality of the window layer and the p/i interface properties in a-$Si_{1-x}O_x$:H single-junction solar cells. The *FF*, a key indicator of window layer quality, was higher in cells with p-a-$Si_{1-x}O_x$:H doped with TMB

and TMB + B_2H_6 compared to cells doped solely with B_2H_6. The TMB and TMB + B_2H_6 cells achieved an *FF* of around 0.70, whereas cells with pure B_2H_6 had a significantly lower *FF* of approximately 0.64.

Overall, the solar cell performance, based on E_{ff}, suggests that p-a-$Si_{1-x}O_x$:H films doped with TMB or TMB + B_2H_6 have superior quality for solar cell applications compared to those doped with pure B_2H_6. Prior studies reported a V_{oc} of 1.0 V for a-$Si_{1-x}O_x$:H solar cells with p-a-$Si_{1-x}O_x$:H window layers. Here, we aimed to further enhance V_{oc} by reducing the H_2/SiH_4 ratio in the absorber layer, while maintaining the TMB + B_2H_6 doping for the window layer. As a result, we achieved a high V_{oc} of 1.0 V, as shown in Figure 9. This experiment indicates that p-a-$Si_{1-x}O_x$:H doped with TMB + B_2H_6 is a promising technique for improving the efficiency of a-Si:H thin-film solar cells.

4. Conclusions

This study explored the impact of various dopant gases, specifically B_2H_6, TMB, and a B_2H_6 + TMB combination, on the optical and electrical properties of boron-doped hydrogenated p-a-$Si_{1-x}O_x$:H films for use as window layers in a-$Si_{1-x}O_x$:H single-junction solar cells. Key findings indicate that TMB-doped films exhibited a higher E_{opt} and better optical properties, while the combined B_2H_6 + TMB doping strategy enhanced conductivity and overall film quality. Films doped solely with B_2H_6 showed lower optical performance, and while their conductivity improved with concentration, they did not match the properties achieved with TMB or the B_2H_6 + TMB mix.

The application of a mixed B_2H_6 + TMB doped p- a-$Si_{1-x}O_x$:H layer in single-junction a-$Si_{1-x}O_x$:H solar cells resulted in the highest efficiency, demonstrating V_{oc} of 1.0 V and an enhanced *FF* due to improved interface quality at the p/i junction. Quantum efficiency measurements confirmed superior short- and long-wavelength light absorption with the mixed doping approach, further supporting its effectiveness in maximizing solar cell performance.

Overall, the use of mixed B_2H_6 + TMB dopants optimizes the balance between electrical and optical properties, yielding higher efficiency and stability in a-$Si_{1-x}O_x$:H thin-film solar cells. This dopant strategy provides a viable pathway for advancing high-performance, low-cost photovoltaic applications, contributing to the broader effort to enhance renewable energy technology.

5. Acknowledgements

This work was supported by National Electronics and Computer Technology Center (NECTEC), Thailand.

6. Authors' Contributions

The first author conducted the experiments, fabricated and characterized the samples, and drafted the manuscript with guidance from the second author, who supervised the project. All authors contributed critical feedback and helped refine the research, analysis, and manuscript.

7. Conflicts of Interest

The authors declare no conflicts interest.

ORCID
Sorapong Inthisang[1] https://orcid.org/0009-0009-0218-8688
Kobsak Sriprapha[2] https://orcid.org/0000-0003-2400-5482

References

Calise, F., Fabozzi, S., Vanoli, L., & Vicidomini, M. (2021). A sustainable mobility strategy based on electric vehicles and photovoltaic panels for shopping centers. *Sustainable Cities and Society*, 70, Article 102891. https://doi.org/10.1016/j.scs.2021.102891

Chen, T.-G., Yu, P., Tsai, Y.-L., Shen, C.-H., Shieh, J.-M., Tsai, M.-A., & Kuo, H.-C. (2012). Nano-patterned glass superstrates with different aspect ratios for enhanced light harvesting in aSi:H thin film solar cells. *Optics Express*, 20(10), A412-A417. https://doi.org/10.1364/oe.20.00A412

Daugaard, D. (2020). Emerging new themes in environmental, social and governance investing: a systematic literature review. *Accounting and Finance*, 60(2), 1501-1530. https://doi.org/10.1111/acfi.12479

Fujikake, S., Ohta, H., Sichanugrist, P., Ohsawa, M., Ichikawa, Y., & Sakai, H. (1994). a-SiO:H films and their application to solar cells. *Optoelectronics - Devices and Technologies*, 9(3), 379-390.

Ichikawa, Y., Fujikake, S., Ohta, H., Sasaki, T., & Sakai, H. (1991). 12% two-stacked a-Si:H tandem cells with a new p-layer structure. In *Proceedings of the 22nd IEEE Photovoltaic Specialists Conference* (pp. 1296-1301). IEEE. https://doi.org/10.1109/PVSC.1991.169417

Kim, G., Lim, J. W., Shin, M. & Yun, S. J. (2018). Bifacial color realization for a-Si:H solar cells using transparent multilayered electrodes. *Solar Energy*, 159, 465-474. https://doi.org/10.1016/j.solener.2017.11.019

Kim, S., Chung, J.-W., Lee, H., Heo, Y. & Lee, H.-M. (2013). Remarkable progress in thin-film silicon solar cells using high-efficiency triple-junction technology. *Solar Energy Materials and Solar Cells*, 119, 26-35. https://doi.org/10.1016/j.solmat.2013.04.016

Kim, Y. K., Guijt, E., Si, F. T., Santbergen, R., Holovsky, J., Isabella, O., van Swaaij, R. A. C. M. M. & Zeman, M. (2015). Fabrication of double- and triple-junction solar cells with hydrogenated amorphous silicon oxide (a-SiOx:H) top cell. *Solar Energy Materials and Solar Cells*, 141, 148-153. https://doi.org/10.1016/j.solmat.2015.05.033

Krajangsang, T., Inthisang, S., Hongsingthong, A., Limmanee, A., Sritharathikhun, J., & Sriprapha, K. (2013). Wide-gap p-μc-Si1-xOx:H films and their application to amorphous silicon solar cells. *International Journal of Photoenergy*, 2013, 1-6. https://doi.org/10.1155/2013/958326

Kumar, P., Kupich, M., Grunsky, D., & Schroeder, B. (2006). Microcrystalline B-doped window layers prepared near amorphous to microcrystalline transition by HWCVD and its application in amorphous silicon solar cells. *Thin Solid Films*, 501(1-2), 260-263. https://doi.org/10.1016/j.tsf.2005.07.151

Lambertz, A., Finger, F., Holländer, B., Rath, J. K., & Schropp, R. E. I. (2012). Boron-doped hydrogenated microcrystalline silicon oxide (μc-SiOx:H) for application in thin-film silicon solar cells. *Journal of Non-Crystalline Solids*, 358, 1962-1965. https://doi.org/10.1016/j.jnoncrysol.2011.12.047

Lim, W. L., Lee, J. D., Lee, S. H. & Yun, J. S. (2014). Cell performance of a-Si:H translucent solar cells with various buffers utilizing light reflected by a backside mirror. *Materials Research Bulletin*, 58, 153-156. https://doi.org/10.1016/j.materresbull.2014.03.016

Macías, J., Herrero, R., José, L. S., Núñez, R., & Antón, I. (2024). On the validation of a modelling tool for vehicle integrated PhotoVoltaics: Reflected irradiance in urban

environments. *Solar Energy Materials and Solar Cells*, 277, Article 113060. https://doi.org/10.1016/j.solmat.2024.113060

Matsumoto, Y., Meléndez, F., & Asomoza, R. (2001). Performance of p-type silicon-oxide windows in amorphous silicon solar cell. *Solar Energy Materials and Solar Cells*, 66(1-4), 163-170. https://doi.org/10.1016/S0927-0248(00)00169-0

Myong, S. Y., Kim, S. S., & Lim, K. S. (2004). Improvement of *pin*-type amorphous silicon solar cell performance by employing double silicon-carbide *p*-layer structure. *Journal of Applied Physics*, 95, 1525-1530. https://doi.org/10.1063/1.1639140

Myong, S. Y., Lee, H. K., Yoon, E., & Lim, K. S. (2002). Highly conductivity boron-doped nanocrystalline silicon-carbide film prepared by low-hydrogen-dilution photo-CVD method using ethylene as a carbon source. *Journal of Non-Crystalline Solids*, 298(2-3), 131-136. https://doi.org/10.1016/S0022-3093(02)00916-X

Otsubo, S., Saito, M., Morimoto, A., Kumeda, M., & Shimizu, T. (1988). a-Si1-xOx:H films prepared by direct photo-CVD using CO_2 gas. *Japanese Journal of Applied Physics*, 27(11A), Article L1999. https://doi.org/10.1143/JJAP.27.L1999

Sánchez, P., Lorenzo, O., Menéndez, A., Menéndez, J. L., Gomez, D., Pereiro, R., & Fernández, B. (2011). Characterization of doped amorphous silicon thin films through the investigation of dopant elements by glow discharge spectrometry: A correlation of conductivity and bandgap energy measurements. *International Journal of Molecular Sciences*, 12(4), 2200-2215. https://doi.org/10.3390/ijms12042200

Schüttauf, J.-W., Niesen, B., Löfgren, L., Bonnet-Eymard, M., Stuckelberger, M., Hänni, S., Boccard, M., Bugnon, G., Despeisse, M., Haug, F.-J., Meillaud, F., & Ballif, C. (2015). Amorphous silicon–germanium for triple and quadruple junction thin-film silicon based solar cells. *Solar Energy Materials and Solar Cells*, 133, 163-169. https://doi.org/10.1016/j.solmat.2014.11.006

Shah, A. V. (2010). *Thin-film silicon solar cells*. EPFL Press. https://doi.org/10.1201/b16327

Sriprapha, K., Sitthiphol, N., Sangkhawong, P., Sangsuwan, V., Limmanee, A., & Sritharathikhun, J. (2011). p-Type hydrogenated silicon oxide thin film deposited near amorphous to microcrystalline phase transition and its application to solar cells. *Current Applied Physics*, 11(1), S47-S49. https://doi.org/10.1016/j.cap.2010.11.008

Staebler, D. L., & Wronski, C. R. (1977). Reversible conductivity changes in discharge-produced amorphous silicon. *Applied Physics Letters*, 31(4), 292-294. https://doi.org/10.1063/1.89674

von Blanckenhagen, B., Tonova, D., & Ullmann, J. (2002). Application of the Tauc-Lorentz formulation to the interband absorption of amorphous semiconductors. *Applied Optics*, 41(16), 3137-3142. https://doi.org/10.1364/AO.41.003137

Wijewardane, S., & Kazmerski, L. L. (2023). Inventions, innovations, and new technologies: Flexible and lightweight thin-film solar PV based on CIGS, CdTe, and a-Si:H. *Solar Compass*, 7, Article 100053. https://doi.org/10.1016/j.solcom.2023.100053

Yadav, R. K., Pawar, P. S., Kim, Y. T., Sharma, I., Patil, P. R., Bisht, N., & Heo, J. (2023). Investigation of hybrid SnSe/SnS bilayer absorber for application in solar cells. *Solar Energy*, 266, Article 112174. https://doi.org/10.1016/j.solener.2023.112174